Polarimetric GNSS-R Sea Level Monitoring using I/Q Interference Patterns at Different Antenna Configurations and Carrier Frequencies

Mahmoud Rajabi, Mostafa Hoseini, Hossein Nahavandchi, Maximilian Semmling, Markus Ramatschi, Mehdi Goli, Rüdiger Haas, Jens Wickert

***Abstract*—Coastal sea level variation as an indicator of climate change is extremely important due to its large socio-economic and environmental impact. The ground-based Global Navigation Satellite System (GNSS) reflectometry (GNSS-R) is becoming a reliable alternative for sea surface altimetry. We investigate the impact of antenna polarization and orientation on GNSS-R altimetric performance at different carrier frequencies. A one-year dataset of ground-based observations at Onsala Space Observatory using a dedicated reflectometry receiver is used. Interferometric patterns produced by the superposition of direct and reflected signals are analyzed using the Least-Squares Harmonic Estimation (LS-HE) method to retrieve sea surface height. The results suggest that the observations from GPS L1 and L2 frequencies provide similar levels of accuracy. However, the overall performance of the height products from the GPS L1 show slightly better performance owing to more observations. The combination of L1 and L2 observations (L12) improves the accuracy up to 25% and 40% compared to the L1 and L2 heights. The impacts of antenna orientation and polarization are also evaluated. A sea-looking Left-Handed Circular Polarization (LHCP) antenna shows the best performance compared to both zenith- and sea-looking Right-Handed Circular Polarization (RHCP) antennas. The results are presented using different averaging windows ranging from 15-minute to 6-hour. Based on a 6-hour window, the yearly Root Mean Square Error (RMSE) between GNSS-R L12 sea surface heights with collocated tide gauge observations are 2.4, 3.1, and 4.1 cm with the correlation of 0.99, 0.982, and 0.969 for LHCP sea-looking, RHCP sea-looking, and RHCP up-looking antennas, respectively.**

***Index Terms*—Global Navigation Satellite Systems-Reflectometry (GNSS-R), Coastal Sea Level Monitoring, Polarimetric GNSS-R, Altimetry, GPS, GNSS, L-Band Remote Sensing, Least-Squares Harmonic Estimation (LS-HE)**

I. Introduction

SEA surface level is a key parameter in many scientific disciplines, including geology, geodesy, oceanography and archaeology which could contribute to recognizing climate and environmental variation. Modern civilization could be affected by major and minor changes in sea surface level due to global warming and natural causes such as floods, tsunami and volcanoes [1]. The information about sea surface level is also vital due to the large population, economic and commercial activities in coastal areas. In addition, sea surface level is essential to defining vertical datum (geoid) and consequently, measuring and understanding Earth's geometric shape. Therefore, it is essential to monitor sea surface level using accurate and reliable methods.

Two prevalent methods have been used for sea level monitoring, traditional tide gauges, and spaceborne radar altimeters. These methods have some limitations. The tide gauge measurements are point-wise and also affected by subsidence, tectonics and human activities [1]. Close to the coastal area, data accuracy of the radar altimeters is degraded due to the effect of the land on its large footprint, and the corrections which are applied for geophysical effects. Consequently, we do not have reliable and accurate spaceborne radar observations in the coastal area besides the limitation on the spatiotemporal resolution of this method [2].

Global Navigation Satellite Systems (GNSS) were designed primarily for providing positioning, navigation, and timing services. The GNSS signals are also being used for numerous remote sensing applications of the Earth's surface and atmosphere, in addition to its primary aim. GNSS-Reflectometry (GNSS-R) as a state-of-the-art remote sensing technique, uses reflected GNSS signals to retrieve and investigate numerous geophysical parameters and phenomena over the Earth's surface (land, ocean, and ice). GNSS-R is a multi-static radar technique in the L-band range of the electromagnetic signals, which works in all weather conditions, day and night, and is ideal for measuring or detecting many variables and natural events, such as sea level [3], sea surface roughness [4], ocean eddies [5], sea ice concentration [6], flood [7], precipitation [8], wind speed [9], and snow depth [10].

Ground-based GNSS-R can act as a multi-purpose sensor, which has drawn attention over the past decades. The method is an alternative option for traditional tide gauges for monitoring sea surface level in coastal areas. A GNSS-R sensor can cover a wider area of the sea surface and collect additional useful data from the reflecting surface, e.g. sea surface roughness and ice coverage. Tide-gauges measurements can be affected by local vertical displacements and require extra procedures to

M. Rajabi, M. Hoseini and H. Nahavandchi are with the Department of Civil and Environmental Engineering, Norwegian University of Science and Technology, 7491 Trondheim, Norway (e-mail: mahmoud.rajabi@ntnu.no).

M. Semmling is with the German Aerospace Center DLR, Institute for Solar-Terrestrial Physics, Neustrelitz, Germany.

M. Ramatschi is with the Department of Geodesy, German Research Center for Geosciences (GFZ), 14473 Potsdam, Germany.

M. Goli is with Faculty of Civil and Architectural Engineering, Shahrood University of Technology, Iran.

R. Haas is with the Department of Space, Earth and Environment, Chalmers University of Technology, Gothenburg, Sweden

J. Wickert is with the Department of Geodesy, German Research Centre for Geosciences (GFZ), 14473 Potsdam, Germany, and also with the Institute of Geodesy and Geoinformation Science, Technische Universität Berlin, Germany

connect the measured relative sea level to the global reference frame. In contrast, coastal GNSS-R stations can monitor and correct the local vertical displacements and provide sea level measurements in the global reference frame. The concept of sea surface level monitoring using GNSS-R was conceived in 1993 [3] and applied for ground-based GNSS-R stations signals in 2000 [11]. Afterward, the performance and reliability of the method have been studied in several cases, e.g. [12, 13, 14, 15, 16, 17, 18].

Most of the ground-based GNSS-R altimetry experiments have used an up-looking geodetic antenna and ordinary surveying receiver based on the Signal to Noise Ratio (SNR) observations of the Global Positioning System (GPS). In addition, various configurations have been considered in different studies in terms of antenna orientation, polarization, and receiver type. For example, Santamaria-Gomez and Watson [19] used three weeks of SNR data in Spring Bay, Australia, from a side-looking GNSS Right-Handed Circular Polarization (RHCP) antenna to improve the SNR altimetry performance compared to a zenith-looking antenna. Padokhin et al. [20] used a four-day dataset obtained from a side-looking and a zenith-looking geodetic antenna to investigate the influence of the antenna layout and the impact of wind waves on GNSS-R altimetry. Alonso-Arroyo et al. [21] utilized three-month data based on a tilted antenna to see how the reflected GNSS signals were affected by coastal sea state. Rodriguez-Alvarez et al. [22] and Hongguang et al. [23] also used a single side-looking antenna for sea level altimetry.

A few studies have utilized dedicated reflectometry receivers with tilted antennas. For example, Semmling et al. [24] use an Occultation, Reflectometry, and Scatterometry (GORS) receiver and reach the Root Mean Squared Error (RMSE) of 35.0 cm for L1 and 47.3 cm for L2 in a sea-ice environment with a 30-min temporal resolution. Liu et al. [25] reports a monthly RMSE of 4.37 cm with respect to tide gauge observations using GPS L1 and a tilted Left-Handed Circular Polarization (LHCP) antenna [25]. The former study uses Doppler residuals being less precise but also less affected by sea state. The latter study uses phase observations during coherent reflection events which limits the measurements to the reflection at low elevation angles or during lower sea states. Fran Fabra et al. [26] used coherent differential phase between direct and both LHCP and RHCP reflected signals for the retrieval of absolute ellipsoidal heights over sea ice. Lifeng Bao et al. [27] to improve precision and spatial resolution of GNSS-R altimetry used one up-looking geodetic GNSS receiver, one downward LHCP antenna, and an atomic clock.

This study aims to give an inter-comparison overview of GNSS-R altimetry observations recorded using different antenna designs and carrier frequencies. Compared to the typical geodetic installations, the tilted antenna orientation coupled with different polarizations strengthens the power of captured interferometric patterns. This can prolong the detectability of these patterns at higher elevation angles. A multivariate spectral analysis method is used here to take the advantage of available concurrent observations. Moreover, the quality of the observations made by each satellite Pseudo Random Noise (PRN) is assessed.

We design different scenarios for the investigation using a dedicated reflectometry receiver under similar conditions, i.e. the same processing method, antenna model, location and weather conditions. The variable parameters in the scenarios are antenna polarizations and orientations, as well as carrier frequency of the signal. The analysis includes the impact of different wind speeds and averaging windows. A relatively long-term dataset from a coastal GNSS-R station with special design and unique features, which is established by the German research center for geosciences (GFZ) is used. The Least-Squares Harmonic Estimation (LS-HE) method is used for spectral analysis and finding the frequency of interferometric signals. The interferometric or compound signal is generated as a result of interference of direct and reflected signals. The frequency observations of the interferometric signals are used to calculate sea surface height. The LS-HE method has the capacity of multivariate formulation and is not limited to integer frequencies and evenly spaced data [28] [29]. The rest of this paper is organized as follows. The study area and dataset are presented in Section 2. The methodology and mathematical concepts are described in Section 3. The discussion of data processing and the results are explained in Section 4. Finally, the paper is finalized by a conclusion in Section 5.

II. Data and site

We use a one-year dataset from January to December 2016 obtained from a dedicated GNSS-R site installed and operated by GFZ. This is one of the two GNSS-R stations at Onsala Space Observatory in Sweden ($57.393^{\circ}N, 11.914^{\circ}E$). The observations with elevation angles between 5 and 40 degrees are selected for the investigation. Besides the GNSS-R observations, we use two ancillary datasets including the wind and sea level measurements from a close by meteorological station and a traditional tide gauge. Both are operated by the Onsala Space Observatory and located at about 300 m distance from the GNSS-R station. Figure 1 shows the study area, reflection points for different PRNs, and a picture of the station antennas and their orientations. A schematic view of the experiment setup and an example of the receiver outputs for satellite PRN 3 during a reflection event is shown in Figure 2.

The station antennas are installed on a concrete foundation with an approximate height of 3 meters from the sea surface. Three types of antennas are installed at the station, one is up-looking and the two others are sea-looking. The up-looking antenna is RHCP and assigns higher gain values to direct GPS signals for acquisition and tracking purposes. The sea-looking antennas with RHCP and LHCP designs are considered for tracking sea reflected GPS signals at two different polarizations. The tilt angle between the up-looking and sea-looking antennas is 98°. Usage of a single side-looking antenna would cause difficulty to continuously track the direct signals due to significant contributions from the reflected signals. Therefore, an upright antenna needs to be used as the master link for the tracking. It should be noted that the side-looking antennas can partially block the reception of reflections in the up-looking antenna. Therefore, the up-looking antenna used at Onsala

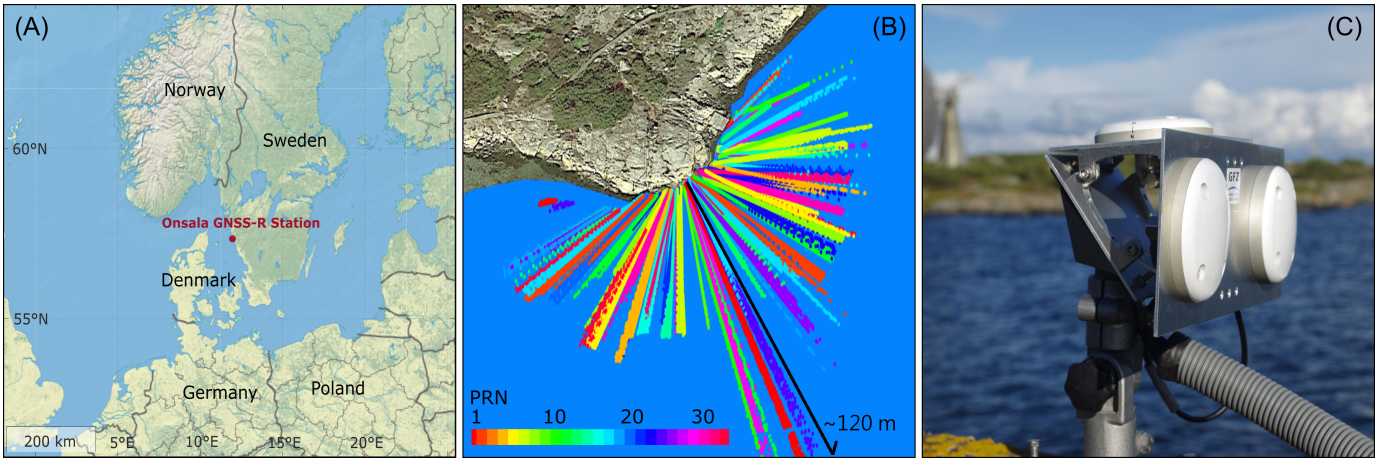

Fig. 1. (A) The red point on the map shows the Onsala GNSS-R station in the southwest of Sweden which the experiment setup is installed there. (B) The scatter plot of the reflection points over the sea surface. The colors show the GPS PRN numbers related to the reflection tracks. (C) The experiment setup and antenna orientations (up- and sea-looking).

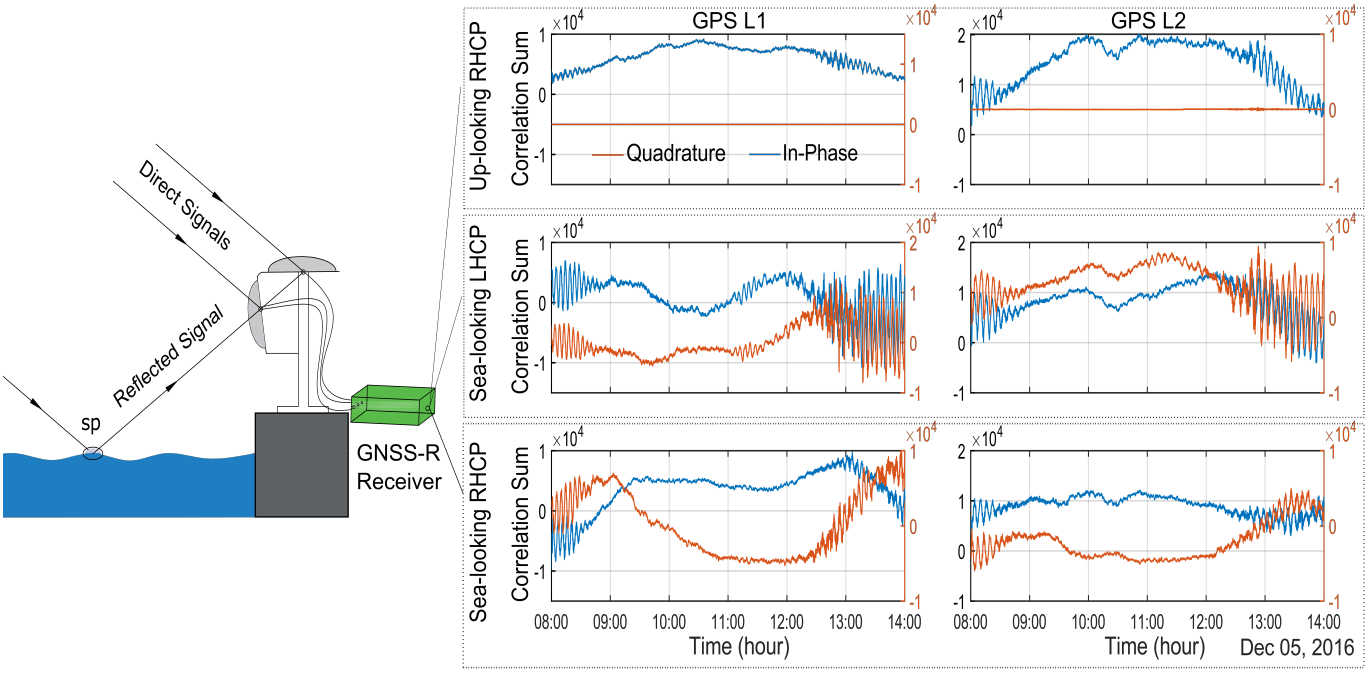

Fig. 2. A schematic view of the GNSS-R experiment setup on the left. The right graphs illustrate example time series of the in-phase and quadrature correlation sums from each antenna in GPS L1 and L2 bands. The graphs are related to a reflection event on December 5, 2016 from the GPS PRN 3. The specular point is denoted by "sp".

station might not provide exactly equivalent configuration compared to a single isolated upright antenna.

A GORS receiver [6] with four antenna inputs is utilized in the experiment. The first input is dedicated to the master channel of the receiver and is connected to the up-looking antenna. The second and third inputs are used for the slave channels and are connected to the sea-looking antennas.

According to [30] the signal processing flow in the dedicated reflectometry receiver can be briefly described as follows (See Figure 3 for a schematic representation of the receiver architecture). The received signal, i.e. $E_d + E_r$ in Figure 3, after digitization in the receiver can be written as:

$$s(t) = A\,D(t-\tau)\,C(t-\tau)\,cos(2\pi(f_{IF}+f_D)t+\varphi) \quad (1)$$

with $s(t)$ being the received signal, A the amplitude, D and C respectively the modulated navigation data and the PRN code, t the time, τ the code delay, f_{IF} an intermediate frequency, f_D the Doppler frequency shift, and φ is an initial phase. The receiver generates the following models of the carrier signal at In-phase and Quadrature (I/Q) levels in the master channels:

$$\text{in-phase}: \qquad \cos(2\pi(f_{IF}+\tilde{f_D})t+\tilde{\varphi})$$

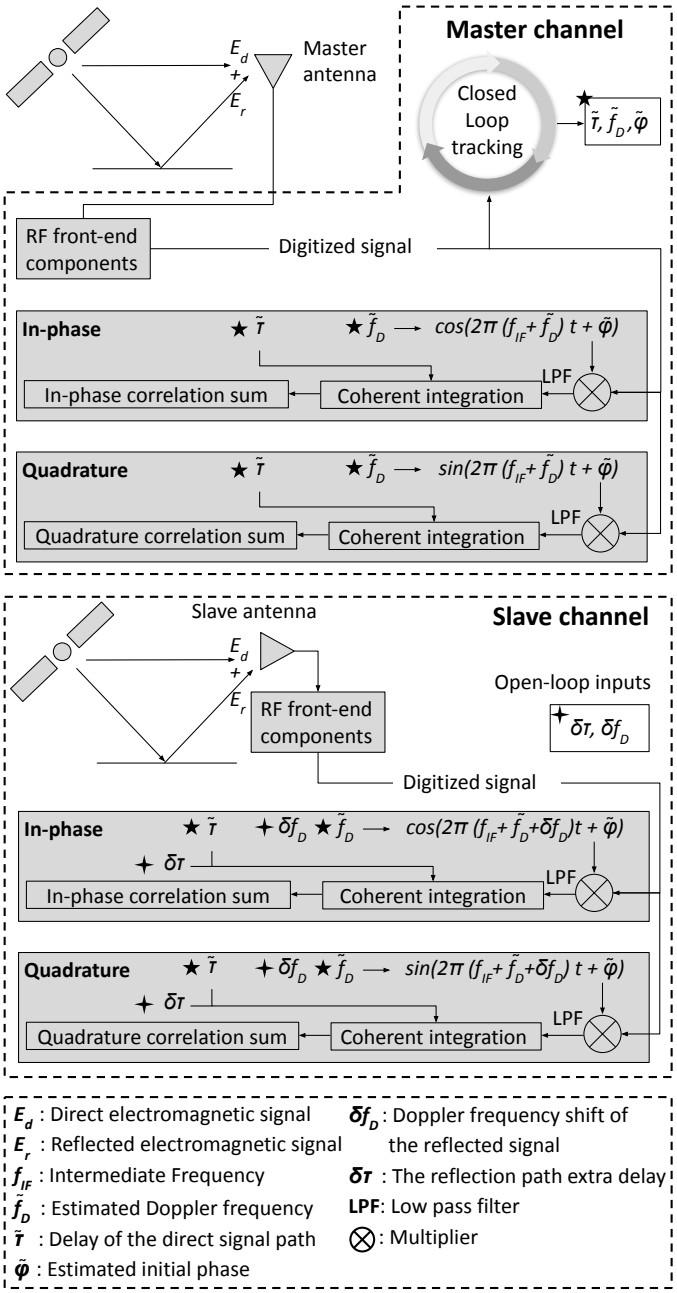

Fig. 3. A schematic diagram of the dedicated GNSS-Reflectometry receiver architecture used in this study.

$$\text{quadrature}: \qquad \sin(2\pi(f_{IF}+\tilde{f_D})t+\tilde{\varphi}) \tag{2}$$

where $\tilde{f_D}$ and $\tilde{\varphi}$ are estimated Doppler frequency and initial phase which are produced by a closed-loop tracking process in the receiver. After multiplying the received signal by the two models and applying a low pass filter, the results are correlated with the PRN code of the satellite. The navigation data is then demodulated to yield a phasor (γ_m) as the output of the master channel [24]:

$$\gamma_m(\tilde{\tau}) \quad = \quad e^{-j\delta\varphi}[A_d + A_r e^{jk\delta\rho}\Lambda(\Delta\tau)] \tag{3}$$

where $\tilde{\tau}$ is the delay of direct signal which is estimated within the closed-loop tracking process, j is the imaginary unit ($j^2 = -1$), $\delta\varphi$ is the phase difference between the compound and direct signals, the amplitudes of the direct and reflected signals are A_d and A_r, respectively, and $k = 2\pi/\lambda$ is the carrier wavenumber with λ being the carrier wavelength. Figure 4 shows a phasor representation of the direct, reflected, and compound signals with the reflectometry angle $\psi = k\,\delta\rho$. The parameter $\Delta\tau$ denotes the time delay due to the excess path ($\delta\rho$) traveled by the reflected signal compared to the direct path. The function $\Lambda(\Delta\tau)$ is triangular auto-correlation function with the properties: $\Lambda(0) = 1$ and $\Lambda(\tau) = \Lambda(-\tau)$. Under successful operation of the phase lock-loop (Fig. 4-B), the amplitude of the signal is completely tracked in the in-phase component of the master channel, I_m [30]. Therefore, the quadrature component of the master channel, Q_m, vanishes and the signal SNR can be calculated by squaring I_m, expressed by:

$$A_c^2 = I_m^2 = A_d^2 + A_r^2 + 2A_dA_r\cos(k\delta\rho) \tag{4}$$

where A_c is the amplitude of the compound signal. The SNR value expressed in (4) is similar to the SNR observations from geodetic receivers described in [31]. The parameter $\delta\rho$ will be later used for the sea level retrieval (see section III).

For the slave channels, the receiver can be steered through an open-loop scheme using external inputs for tracking the signals intercepted by the slave antennas. The external inputs, δf_D and $\delta\tau$, are relative values with respect to the reference values $\tilde{\tau}$ and $\tilde{f_D}$. The parameter δf_D is used during carrier wipeoff and $\delta\tau$ for the code correlation in the slave channel. The slave channel output can be expressed by:

$$\begin{aligned}\gamma_s(\tilde{\tau}+\delta\tau) \quad &= \quad e^{-j\,(\delta\varphi+\varepsilon_d)}[A'_d\,\Lambda(\delta\tau) + \\ &\qquad A'_r\,e^{j\,(k\,\delta\rho+\varepsilon_d-\varepsilon_r)}\,\Lambda(\delta\tau-\Delta\tau)]\end{aligned} \tag{5}$$

where subscript s refers to the slave channels. The baseline between the master and slave antennas and different carrier phase wind-up for the up-looking and side-looking antennas introduce some phase residuals which are included in ε_d and ε_r for direct and reflected signals, respectively. A'_d and A'_r are respectively the amplitudes of direct and reflected signals in the slave channel. The amplitudes of direct and reflected signals are different in the master and slave channels, mainly because of the different antenna gains. Figure **??** shows a simplified phasor representation of direct, reflected, and compound signals in the slave channel.

The low reflector height at the Onsala GNSS-R station with respect to the sea surface results in $\delta f_D \approx 0$ and $\delta\tau \approx \Delta\tau \approx 0$. Therefore, the receiver outputs for the slave channels at I/Q levels can be simplified to:

$$\begin{aligned}\gamma_s \quad &= \quad A'_c\,e^{j\Delta\varphi} = I_s + jQ_s \\ &= \quad e^{-j(\delta\varphi+\varepsilon_d)}[A'_d + A'_r\,e^{j\,(k\,\delta\rho+\varepsilon_d-\varepsilon_r)}]\end{aligned} \tag{6}$$

where $\Delta\varphi$ is the slave-master phase difference and A'_c is the amplitude of the compound signal in the slave channel. The I/Q components of the slave channel output can be written as:

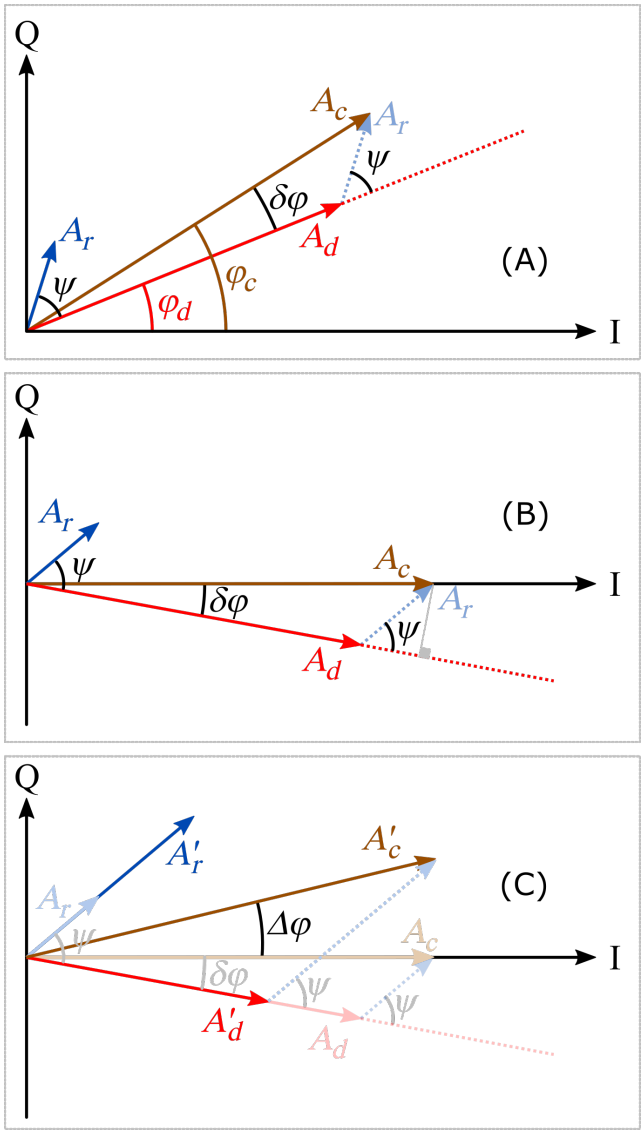

Fig. 4. A phasor diagram of direct, reflected, and compound signals in the master channel respectively denoted by subscript d, r, and c in the in-phase/quadrature (I/Q) axes before (A) and after (B) tracking the phase of the compound signal. The angle ψ is the reflectometry-relevant phase. $\delta\varphi$ is the phase difference between the compound and direct signals.

$$\begin{aligned} I_s &= A'_d \cos(\delta\varphi + \varepsilon_d) + A'_r \cos(k\,\delta\rho - \delta\varphi - \varepsilon_r) \\ Q_s &= -A'_d \sin(\delta\varphi + \varepsilon_d) + A'_r \sin(k\,\delta\rho - \delta\varphi - \varepsilon_r) \end{aligned} \quad (7)$$

The first terms of (7) are related to the contribution of the direct signal while the second terms comprise the effect of the reflected signal:

$$\begin{aligned} I_s &= I_d + I_r \\ Q_s &= Q_d + Q_r \end{aligned} \quad (8)$$

The direct signal terms, i.e. I_d and Q_d, can be extracted e.g. by fitting a low-order polynomial. The amplitude and frequency of the interferometric patterns in the reflected signal terms, i.e. I_r and Q_r, can be determined through different spectral analysis or modeling methods. The LS-HE method, which is further described in the next section, can simultaneously model the direct signal effects and retrieve period of the interferometric oscillations from the I/Q samples. The amplitude of the direct, reflected, and compound signals in the slave channels can be respectively calculated by:

$$\begin{aligned} A'^{\,2}_d &= I_d^2 + Q_d^2 \\ A'^{\,2}_r &= I_r^2 + Q_r^2 \\ A'^{\,2}_c &= I_s^2 + Q_s^2 \\ &= A'^{\,2}_d + A'^{\,2}_r + 2A'_d A'_r \cos(k\delta\rho + \varepsilon_d - \varepsilon_r) \end{aligned} \quad (9)$$

The original output of the GORS receiver is based on 5-millisecond coherent integration, i.e. 200 Hz sampling rate. In this study, the 200 Hz correlation sums are down-sampled using a 10-second (0.1 Hz) integration at I/Q levels for each of the antennas.

In general, having access to the I/Q outputs gives the opportunity of looking at the signal in a 3D sense and retrieving the phase of interferometric signal and the coherence state [25]. In this study, we directly utilize the I/Q outputs. Both of the components encompass the oscillating interferometric patterns regardless of the coherency of the reflection. This feature in both of the I/Q components is used here to detect the corresponding Doppler residual in a multivariate approach as described below.

III. Method

The methodology of this study contains three main stages (Fig. 5). The first stage is the data preparation through which the time series associated with each reflection event are created. In the second stage, we focus on finding the interferometric frequency using multivariate LS-HE in different scenarios. The frequency (L1/L2) and polarization (RHCP/LHCP) of the reflected signals as well as the orientation of the antenna (up-/sea-looking) are variable factors in these scenarios.

Four main scenarios for the estimation of the sea surface heights are designed as follow, each one using L1 and L2 separately: (A) using the I components of the up-looking RHCP antenna (one time series), (B) using the I/Q components of the sea-looking RHCP antenna (two time series), (C) using the I/Q components of the sea-looking LHCP antenna (two time series), (D) using the I/Q components of the both sea-looking antennas (four time series). In addition, the sea surface heights are estimated by combining the retrieved heights from L1 and L2 for each main scenario for possible improvement. Consequently, the sea surface heights are retrieved in 12 different solutions. These products make it possible for us to assess the performance of polarimetric GNSS-R in different antenna's angle plus the performance of L1, L2, and combination of them (L12). The parameter of interest in the LS-HE analysis is the period of the interferometric signals.

The time series of the reflection events are divided into smaller segments by considering a time window. The time

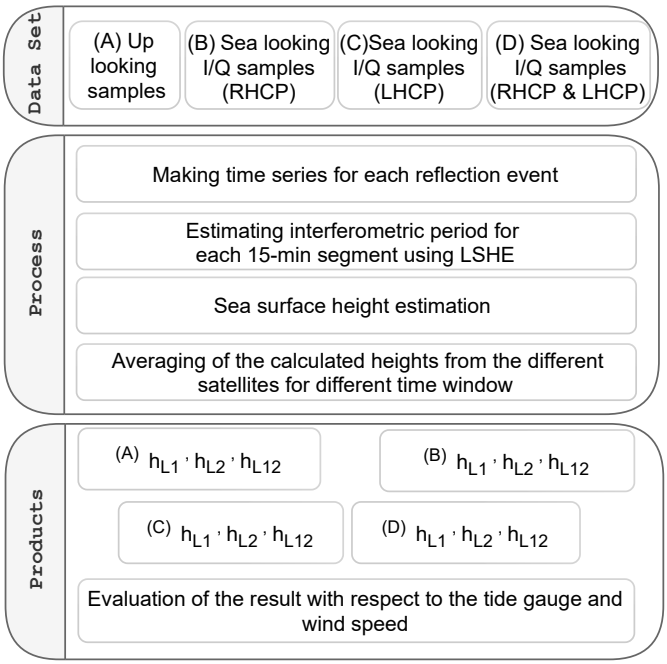

Fig. 5. Methodology flowchart based on the Least Squares Harmonic Estimation (LS-HE).

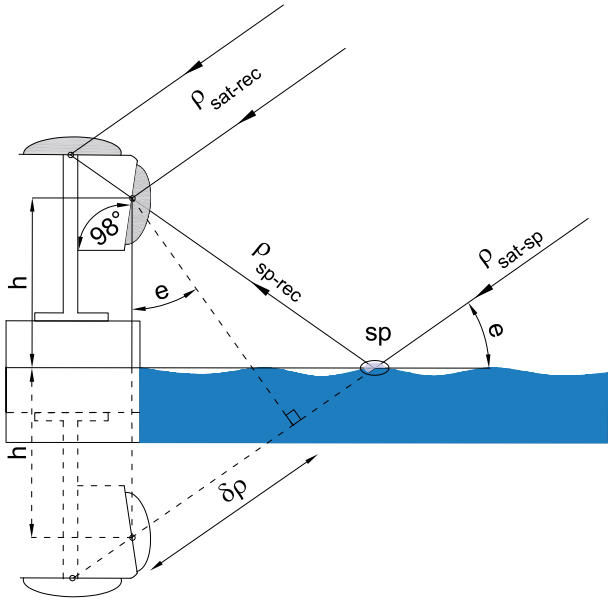

Fig. 6. Schematic geometry of the ground-based GNSS-R altimetry based on the path difference between the direct and reflected satellite signals. ρ_{sat-sp} is the distance between the satellite and specular point, $\rho_{sat-rec}$ is the distance between the satellite and receiver antenna, ρ_{sp-rec} is the distance between the specular point and receiver antenna, e is the satellite elevation angle, $\delta\rho$ is the extra path of the reflected signal compared to the direct signal, and h is the height difference between the phase center of the antenna and sea surface.

window for retrieving this periodic pattern is set to a minimum of 15 min but it is flexibly extended to 30 min until it includes at least two interferometric periods. It is worth mentioning that higher antenna height with respect to the sea surface could have reduce this window size resulting in a better temporal resolution. We move the overlapping window and analyze the segment with a time step of 1-min to cover the whole time series. The sea surface height is estimated from each segment.

To combine the estimated heights from different satellites we use an averaging window. For outlier detection, we use a native MATLAB function that utilizes the median absolute deviation (MAD) values. All the values beyond three scaled MAD with respect to the median are considered as outliers. After outlier elimination, the median value of the estimates within the averaging window is considered as the final height estimate. The final estimates are calculated every 5 minutes with different averaging windows ranging from 15 minutes to 6 hours (6-hours, 3-hours, 1-hours, and 15 minutes). The last stage of the methodology is the validation of the GNSS-R height estimates with the collocated tide gauge observations at different wind speeds.

A. Least-Squares Harmonic Estimation (LS-HE)

The LS-HE is one of the frequency analysis methods from the generation of the Fourier spectral analysis. The method is restricted to neither integer frequencies nor evenly-spaced time series and can be applied to datasets with gaps. The LS-HE method can efficiently include a linear trend as a deterministic part of the model and the covariance matrix as the stochastic part of the model [28]. One important feature of the method compared to the least squares spectral analyses described by earlier studies e.g. [32, 33, 34] is the multivariate formulation to identify common-mode signals of multiple time series. This feature has been utilized in scenarios B, C, and D to enhance retrieval of the common interferometric signal. For scenario A which includes only one time series, the analysis becomes univariate. The LS-HE method was presented and utilized by [35] for the GPS position time series and here is introduced for GNSS-R altimetry. For more information about the theory of LS-HE, we may refer to [36] [37].

B. Sea surface height calculation

The superposition of direct and reflected signals constructs compound signals. The concept of calculating the sea surface height from the GNSS-R observations is based on the retrieval of the interferometric patterns in the compound signal. The LS-HE method used in this study includes individual linear terms for each of the I/Q components of the master or slave samples. These linear terms can absorb the effect of direct signal variations (see (7)). Therefore, the effect of direct signal and interferometric oscillations can be effectively separated within the LS-HE analysis. The estimated interferometric period by LS-HE can then be related to the geometry of the reflection as described below.

The difference between the direct and reflected signals paths creates a Doppler shift which is in fact the frequency of the interferometric fringes [6]:

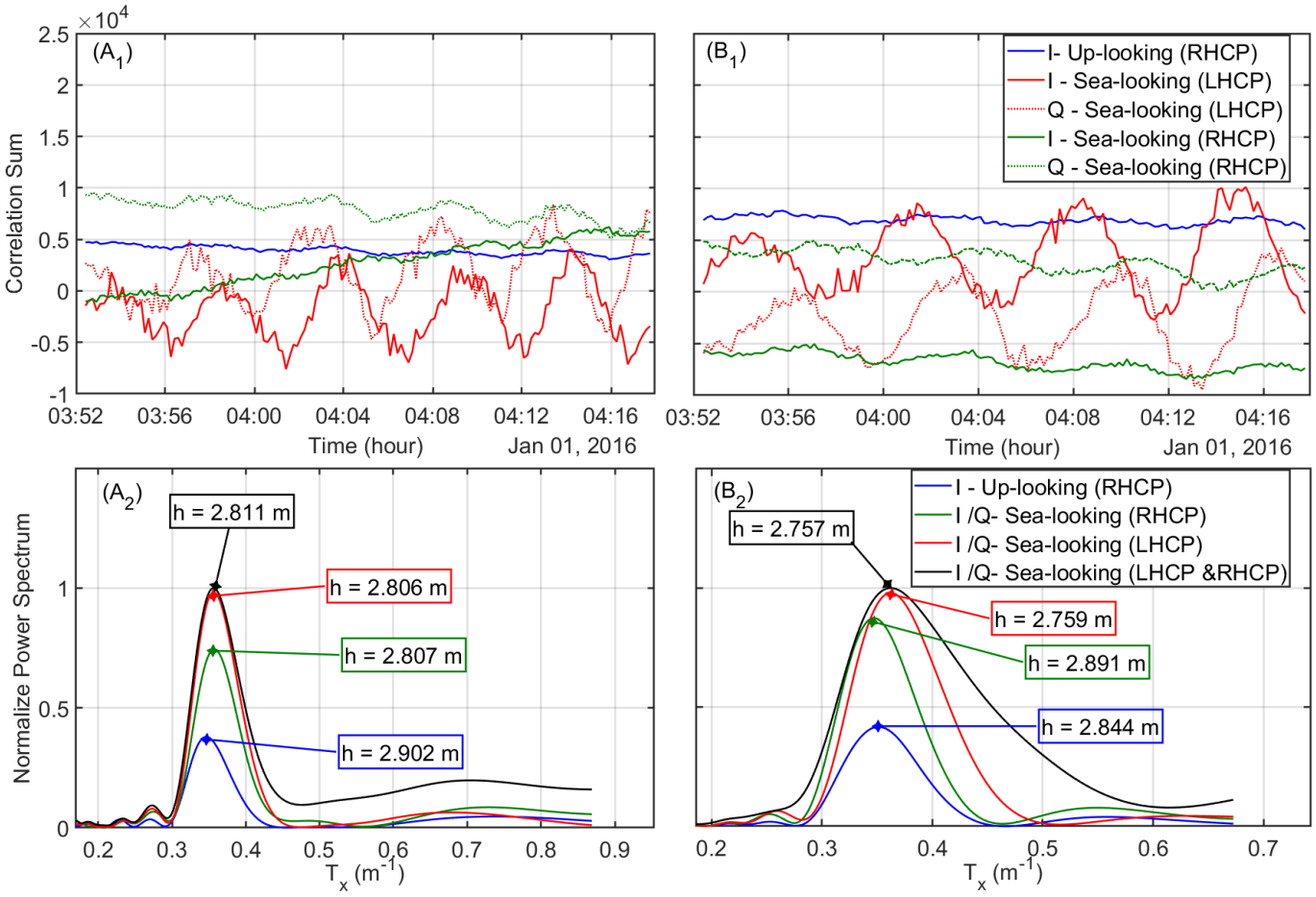

Fig. 7. Examples of observation time series of PRN 26 for one segment which are used to retrieve interferometric period (T_{int}) using multivariate LS-HE formulation. (A_1) and (B_1) show the In-phase and Quadrature components for GPS L1 and L2, respectively. (A_2) and (B_2) illustrate the dominant interferometric period retrieved by LS-HE based on different combinations of the time series.

$$\delta f = \frac{1}{\lambda}\frac{d(\delta\rho)}{dt} \quad (10)$$

$$\delta\rho = \rho_{ref} - \rho_{dir}, \quad (11)$$

where ρ_{dir} and ρ_{ref} are the distance between the satellite and the antenna for direct and reflected signals, respectively, δf is the Doppler shift, and λ is the wavelength of the signal carrier. As shown in Figure 6, $\delta\rho$ can be estimated by:

$$\delta\rho = 2\ h\ sin(e) \quad (12)$$

where e is the satellite elevation angle, h is the height difference between the phase center of the antennas and sea surface. Let us introduce the variable $x = 2\sin(e)/\lambda$. The interferometric frequency with respect to x denoted by δf_x can be retrieved by:

$$\delta\rho = \lambda\, h\, x$$

$$\delta f_x = \frac{1}{\lambda}\frac{d(\delta\rho)}{dx} = h + x\frac{dh}{dx} = h + x\,\dot{h}\,\frac{dt}{dx} \quad (13)$$

with $\dot{h} = dh/dt$ being the height rate. To account for the height rate in the height retrieval process, we first calculate a sea level estimate using the detected interferometric period (T_{int}) in the LS-HE analysis:

$$P(T_x) = LSHE(x, Y)$$

$$\{P_{max}, T_{int}\} = max[P(T_x)]$$

$$h \approx \delta f_x = \frac{1}{T_{int}} \quad (14)$$

where $P(T_x)$ is the power spectrum, Y is the matrix of observations, P_{max} is the detected maximum power using the max function. The columns of Y for each scenario include the following time series:

$$\begin{aligned}
&\text{Solution A:} \quad Y = [I_m^2] \\
&\text{Solution B:} \quad Y = [I_s^R, Q_s^R] \\
&\text{Solution C:} \quad Y = [I_s^L, Q_s^L] \\
&\text{Solution D:} \quad Y = [I_s^R, Q_s^R, I_s^L, Q_s^L]
\end{aligned} \quad (15)$$

with superscript R and L denoting the RHCP and LHCP sea-looking antennas. Having the sea level estimate h from the LS-

HE analysis and $\dot{h} = 0$ as the initial value, we find final values of h and $\dot{h}$ through iterative minimization of the following cost function:

$$\min_{h,\dot{h}} \sum_{i}^{N} \|\hat{Y}_i - a_i \sin(\frac{4\pi[h + \delta h] \sin(e)}{\lambda} + \phi_i)\| \tag{16}$$

$$\delta h = \frac{\dot{h} \tan(e)}{\dot{e}} \tag{17}$$

where δh is a correction term to compensate the height rate effect, $\dot{e}$ is the elevation angle rate, $\hat{Y}_i$ is the *i*-th observation time series after removing the linear trend, N is the number of observations processed by LS-HE which is 1 in scenario A, 2 in scenarios B and C, and 4 in scenario D, a_i and ϕ_i are the amplitude and phase offset of the interferometric signal in the *i*-th observation time series that are estimated by least squares analysis.

It should be noted that the side-looking outputs might be contaminated by small phase differences. Two possible causes can be antenna phase center variations [25] and the offset vectors between the master and slave antennas shown in Fig. 6. These effects can introduce low-frequency components to the I/Q outputs. However, at this station these components have much lower frequency compared to the prominent interferometric fringes [4] and would not significantly affect our sea level measurements.

IV. Results and Discussion

A. Data preparation

The data preparation starts with selecting valid observations which include reflected signals from the sea surface. For this purpose, the precise location of the specular points is estimated within a ray tracing algorithm described by [38] which considers earth surface curvature. A spatial mask using a polygon is then created and applied to the observations to keep the specular points on the sea surface and filter out the reflections from land. To decrease atmospheric effect observations with elevation angles below 5 degrees are excluded. The remaining atmospheric effect is neglected due to the low reflector height. The receiver position is calculated by precise analysis of the direct signals using broadcast ephemerides for the satellite position. The Earth Gravitational Model (EGM96) is used as a reference height. For more information we may refer to [24]. Figure 1-B illustrates the sea-reflected specular points for different GPS satellites used in this study.

B. Applying the LS-HE

For utilizing the LS-HE method, we use a numerical search to catch the dominant interferometric signals in each segment. The step size for searching the interferometric periods is small for the lower periods and gets larger at higher periods using the following recursive formula:

$$T_i = T_{i-1}(1+\alpha \frac{T_{i-1}}{T_{max}}) \ , \ \alpha = 0.01 \ , \ i = 1, 2, ..., T_i \leq T_{max}, \tag{18}$$

where T_i are the trial periods, T_0 and T_{max} are the minimum and maximum detectable periods in the time window of the segments based on the Nyquist's theorem and the α coefficient allows us to make the initial step bigger and smaller for frequency searching. We assume the covariance matrix is the Identity matrix $Q_y = I$ for each time series.

Figure 7 shows an example outcome of the LS-HE on the time series which is generated from a segment of one event for satellite PRN 26 in L1 and L2 bands. Figure 7-A_1 and B_1 show the I and Q components from each antenna and frequency. Figure 7-A_2 and B_2 depict the results of frequency analysis based on the four scenarios for L1 and L2. As can be recognized from the frequency analysis results in the figure, the highest power of the interferometric period belongs to multivariate analysis of time series of both sea-looking antennas. Slightly lower power can be seen for the time series of the LHCP sea-looking antenna.

C. GNSS-R height retrieval and evaluation

The RMSE values of GNSS-R height estimates from the time series of 31 GPS satellites based on different antenna configurations are summarized in Fig. 8. The heights are estimated using the median of each PRN's observations over a 6-hour window and are compared to tide gauge measurements. The RMSE values shown in this figure are related to individual performance assessments of each satellite. The analysis shows that changing the orientation of the antenna towards the reflecting surface can improve Accuracy. This can be recognized by relatively smaller errors in the estimated heights from the sea-looking RHCP antenna (Fig. 8-A) compared to the up-looking RHCP antenna (Fig. 8-B). The sea-looking LHCP antenna (Fig. 8-C), however, shows a better accuracy compared to the sea-looking RHCP antenna. The fully polarimetric solution, i.e. by the combination of the LHCP and RHCP sea-looking antennas, exhibits the best performance with more consistency between the L1 and L2 measurements and over all the PRNs. Discrepancies in the performance of different PRNs shown in Fig. 8 might be related to various factors including the performance of the antennas in different azimuth angles in terms of phase center variations and antenna gain, as well as satellites Equivalent Isotropically Radiated Power (EIRP) variations. In the next step, we retrieve the final sea level products by combining the observations from all the satellites.

The polarization of the antenna can also affect the GNSS-R height estimation. This can originate from the strength of the reflected signals in different polarizations. The direct GNSS signals with RHCP design will have both RHCP and LHCP components after reflection. The strength of these components can be calculated from Fresnel equations and are functions of the elevation angle of satellites and permittivity of the reflecting surface. The power loss due to reflectivity of seawater at Onsala station [4] suggests that the RHCP component is the dominant component at very low elevation angles. The strengths of the RHCP and LHCP components are almost the same at the elevation angle of about 7 degrees. For higher elevation angles the LHCP component is the predominant part of the signal. Therefore, the LHCP antenna can capture

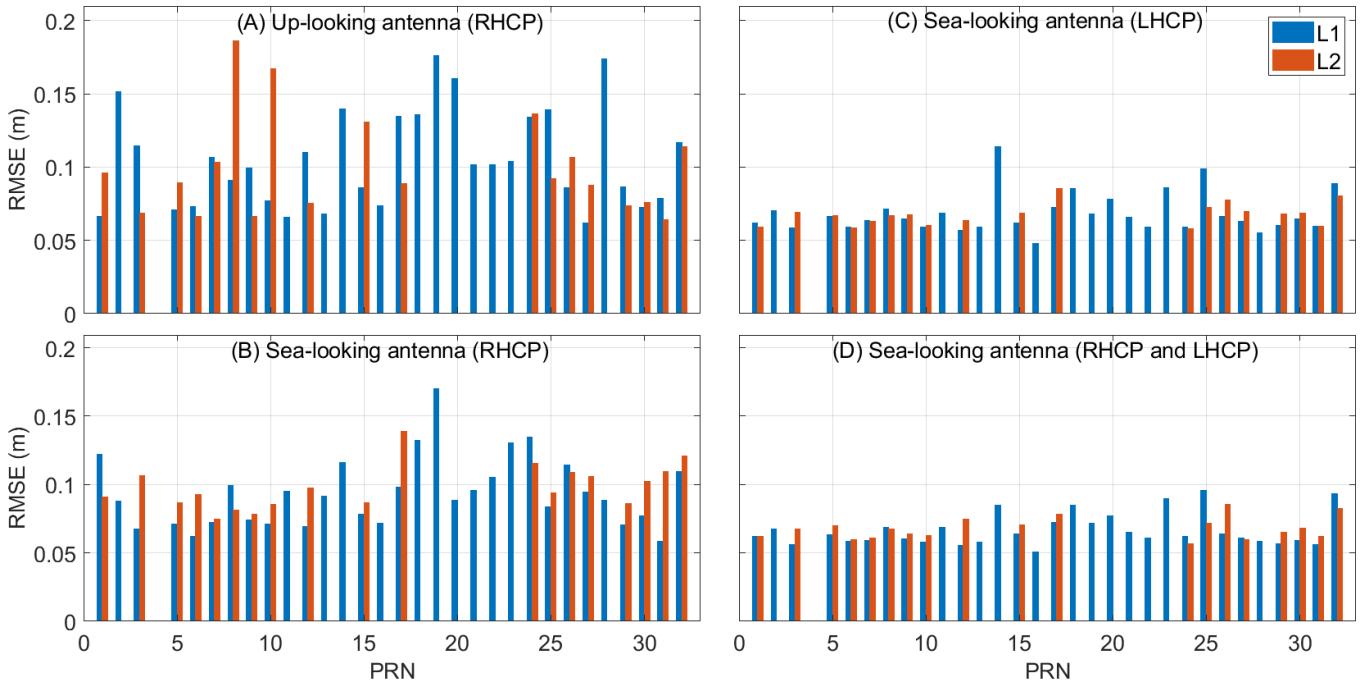

Fig. 8. The Root Mean Squared Error (RMSE) values based on the comparison of GNSS-R sea surface heights with the tide gauge measurements for each GPS Pseudo Random Noise (PRN) numbers from A) up-looking antenna with Right-Handed Circular Polarization (RHCP), B) sea-looking RHCP antenna, C) sea-looking Left-Handed Circular Polarization (LHCP) antenna, and D) combined sea-looking RHCP and LHCP antennas. The red bars are RMSE values of the L2 retrieved heights and the blue bars belong to the L1 retrieved heights. The empty L2 bars are related to the GPS IIR satellites block which do not transmit the L2C signal. The time step and the averaging window for calculating the heights are 5-min and 6-h.

stronger reflections at higher elevation angles. This provides improved performance for retrieving interferometric periods from the LHCP time series (Fig. 8-C). The combination of retrievals from the RHCP and LHCP antennas provide the best performance as can be seen from Fig. 8-D.

Figure 9 presents estimated sea surface height anomalies, using the described method based on the scenarios A, B, C, D. The anomalies are the sea surface heights minus their mean value calculated separately for each solution. The collocated tide gauge measurements are overlaid for comparison. The left panels show the results for the whole dataset (one year) and the right panels illustrate a closer look over a time span of 2 days. As shown in the figure, in all of the four scenarios, the height estimates from the combination of L1 and L2 observations (L12), closely follow the tide gauge measurements. The height retrievals from the L1 observations show almost similar performance compared to L12, although the L1 results from both of the sea-looking antennas show noticeable improvements with respect to the up-looking antenna. The quality of the height measurements from the L2 observations are slightly degraded compared to the L1 and L12 measurements, especially for the RHCP antennas. Considering the fact that not all GPS satellites transmit L2C signal, the lower quality of L2 observations in RHCP antennas can adversely impact the final height retrievals.

We evaluate the final height results using the RMSE values of the GNSS-R measurements with respect to the collocated tide gauge. The correlation values of the GNSS-R and tide gauge measurements are also calculated. Table I shows the RMSE and correlation values based on the described scenarios and four different time windows. The height estimates from the combination of the L1 and L2 observations (L12) provide the best accuracy and robustness. The L12 solution can improve the results up to 25% and 40% compared to the L1 and L2, respectively. The results from L1 observations provide the closest accuracy with respect to the L12 results. Figure 10 is a visualization of Table I . As seen in the table and figure the best accuracy is achieved with the 6-hour window in the mode of L12 using either LHCP antenna or the combination of the two sea-looking antennas. The results for the combination of the sea-looking antennas in L12 mode is 2.3, 3.0, 4.5, and 5.6 cm for the window size of 6, 3, 1 hour, and 15 minutes.

The overall improvement of the RHCP sea-looking antenna compared to the RHCP up-looking antenna in L2 observations is smaller compared to the L1 results. Despite the fact that the combination of sea-looking RHCP and LHCP antennas for each GPS PRN improves the corresponding accuracy (Fig. 8), the final sea level products from the sea-looking LHCP antenna (Fig. 10-C) shows almost the same performance compared to the combined solution (Fig. 10-D). The earlier inter-comparison study conducted by [17] at another GNSS-R station at Onsala has reported to have an RMSE range of 2.6 to 8.1 cm based on four different SNR-based methods and the window size of 6 to 8 hours. Compared to our

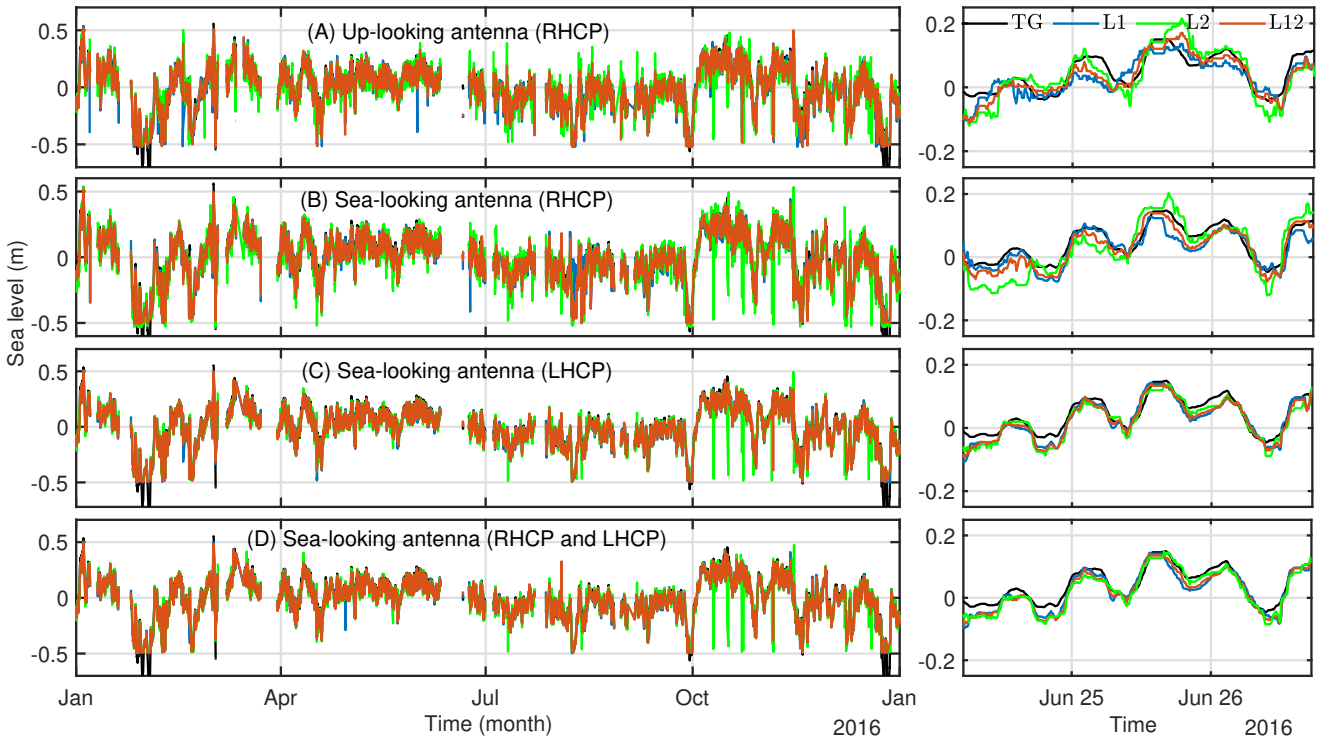

Fig. 9. Time series of sea surface height anomalies derived from GNSS-R observations at Onsala station for the year 2016 (left panels), and closer looks over a period of 2 days (right panels), overlaid on the collocated tide gauge measurements. The height measurements are estimated based on the GNSS-R observations from (A) the up-looking RHCP antenna, (B) the sea-looking RHCP antenna, (C) the sea-looking LHCP antenna, and (D) both sea-looking antennas. The black graph shows the tide gauge measurements, the blue, green, and red colors are the GNSS-R height estimates from the L1, L2, and combined L1 and L2 (L12) sea surface heights. The time step and the averaging window for calculating the heights are 5-min and 6-h.

study,¨the second GNSS-R station uses a geodetic receiver and an up-looking antenna with approximate height of 4 meters from the sea surface.

Wind speed is one of the parameters which affects the accuracy of the sea surface altimetry due to the change of the sea surface roughness. To assess the impact of wind on the accuracy of the estimated sea surface heights, the data are divided based on the Beaufort wind force scale, which is an empirical scale related to wind speed and observed conditions at sea or land. The right panels of Fig. 11 show the yearly RMSE values of the retrieved sea surface heights compared with tide gauge in different Beaufort wind force scale for solution C and D. The heights are estimated in 5-min time step and 6-h averaging window. As seen in the figure with the increase of the wind speed the accuracy degrades. This effect is more pronounced in the products related to L2 signals. Overall, the fully-polarimetric solution (D) shows slightly better performance compared to solution C. The left and middle panels of the figure also present the scatter plots of the GNSS-R sea surface height changes compared to the tide gauge sea level variations. As seen in the figure the distribution of the data in L1 and L12 height measurements are better than L2. Moreover, the number of outliers in the L2 products are more than L1 and L2. Most of the outliers show a correlation with the wind speed in all of the three modes. Generally, the results show excellent agreement with the tide gauge measurements in terms of the correlation and distribution. The solid red and dashed black lines respectively show the fitted linear line and 1:1 ideal correlation. The best agreement is related to L12 retrieved heights.

V. Summary and Conclusion

The study presents the results of sea level measurements using the reflected signals of the Global Navigation Satellite Systems (GNSS) from a coastal experiment at the Onsala Space Observatory in Sweden. The GNSS-Reflectometry (GNSS-R) experiment is equipped with three antennas with different polarizations and orientations. The measurements are calculated based on the application of the Least-Squares Harmonic Estimation method to a dataset of one year over 2016. Based on the flexible configuration of the experiment setup, the effects of polarization, antenna orientation, and the frequency of the GNSS signals are investigated and discussed. The dataset is accompanied by two collocated datasets from the nearest meteorological and tide gauge stations.

Our analysis shows that the best performance can be achieved by a combination of observations from L1 and L2 frequencies (L12) recorded by a sea-looking Left-Handed Circular Polarization (LHCP) antenna. Turning the antenna orientation towards the sea, i.e. a tilt angle of about 90 degrees

TABLE I: The yearly Root Mean Squared Error (R) and the correlation (C) values of GNSS-R sea surface heights with tide gauge measurements based on four averaging windows, two antenna orientations (up-looking and sea-looking), and two polarizations, i.e. Right- and Left-Handed Circular Polarization (RHCP and LHCP). Subscript A, B, C, and D indicate the results from the up-looking RHCP antenna, sea-looking RHCP antenna, sea-looking LHCP antenna, and combination of both sea-looking antennas, respectively. $L1$, $L2$, and $L12$ respectively represent the sea level results of $L1$, $L2$, and combination of $L1$ and $L2$ height measurements (in the averaging step).

Win = 6 h	**L1**	**L2**	**L12**
R_A (cm)	4.6	5.7	4.1
C_A	0.963	0.943	0.969
R_B (cm)	4.2	5.7	3.1
C_B	0.968	0.948	0.982
R_C (cm)	2.4	3.6	2.4
C_C	0.990	0.977	0.99
R_D (cm)	2.4	3.8	2.3
C_D	0.990	0.973	0.990
Win = 3 h			
R_A (cm)	6.1	7.8	5.7
C_A	0.940	0.901	0.946
R_B (cm)	5.3	7.1	4.4
C_B	0.951	0.923	0.967
R_C (cm)	3.2	4.0	3.0
C_C	0.982	0.972	0.984
R_D (cm)	3.1	4.2	3.0
C_D	0.983	0.970	0.984
Win = 1 h			
R_A (cm)	8.6	10.4	8.14
C_A	0.893	0.847	0.901
R_B (cm)	7.4	9.1	6.6
C_B	0.912	0.884	0.930
R_C (cm)	4.7	5.3	4.5
C_C	0.964	0.954	0.967
R_D (cm)	4.6	5.4	4.5
C_D	0.965	0.952	0.967
Win = 15 min			
R_A (cm)	11.7	12.1	10.3
C_A	0.827	0.811	0.854
R_B (cm)	9.3	10.9	8.7
C_B	0.870	0.846	0.886
R_C (cm)	5.8	6.4	5.6
C_C	0.946	0.935	0.949
R_D (cm)	5.6	6.3	5.6
C_D	0.948	0.837	0.949

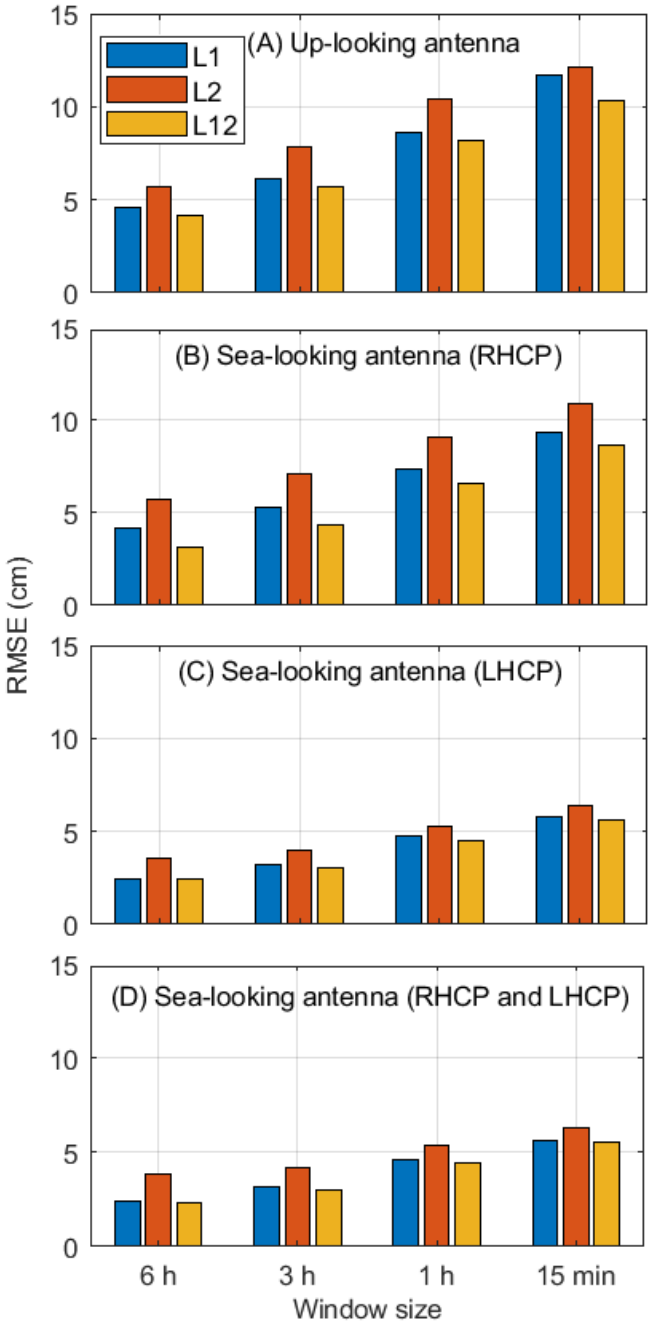

Fig. 10. The annual RMSE values of the GNSS-R sea surface height with respect to the tide gauge measurements for up-looking and sea-looking antennas in four types of window size to average sea surface heights.

with respect to the zenith, maximizes the gain of the antenna for capturing the reflections and thus stronger interferometric patterns. The seaward orientation can improve the accuracy of RHCP sea level results up to 20%, 13%, and 25% respectively for L1, L2, and L12. This improvement can reach about 48%, 50% and 47% for L1, L2, and L12 if the tilted antenna

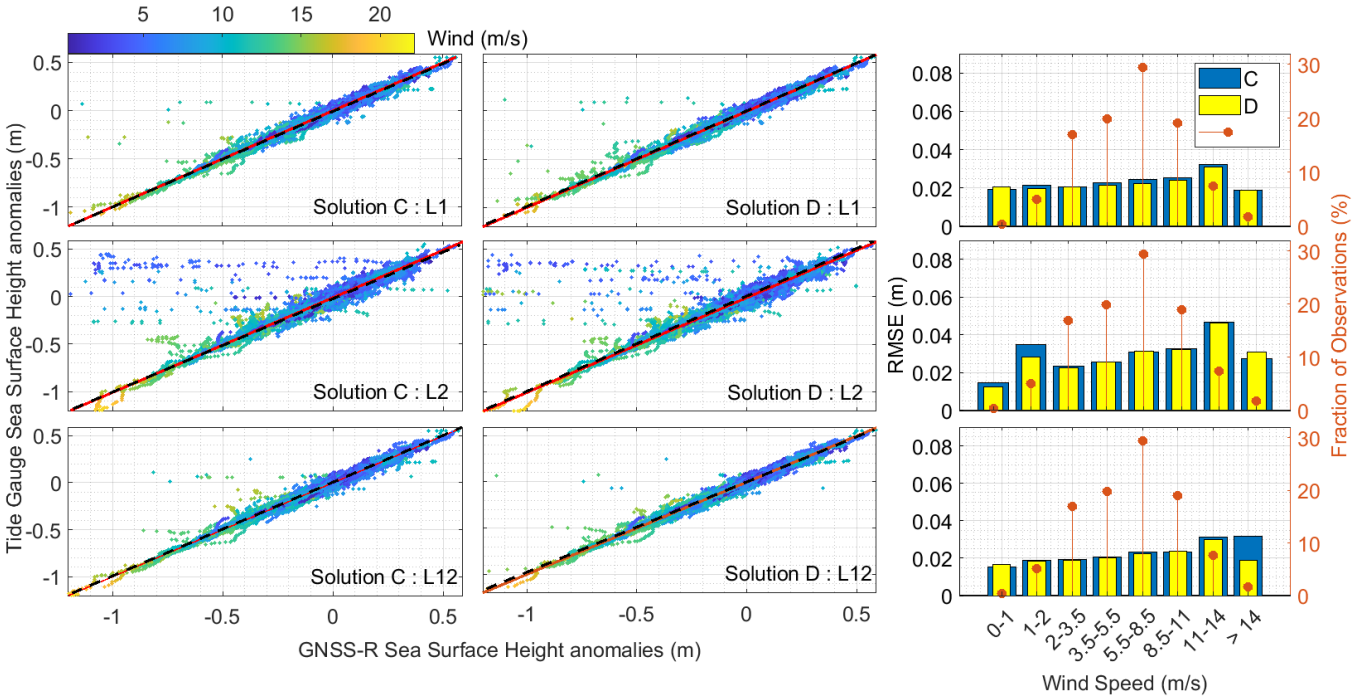

Fig. 11. The left and middle panels illustrate the scatter plots of the GNSS-R height anomalies and tide gauge height anomalies with respect to the wind speed. The graphs are related to the solutions C and D for L1, L2, and the combination of them (L12). The time step and the averaging window for calculating the heights are 5-min and 6-h. The fitted line and 1:1 ideal correlation are shown by the solid red line and dashed black line, respectively. The right panels show the RMSE values between the obtained GNSS-R heights and tide gauge measurements overlaid by the fraction of the data in red bars.

is LHCP. The accuracy supremacy of LHCP measurements compared to the RHCP measurements can be attributed to the stronger reflections from the seawater at LHCP. Except for very low elevation angles, the LHCP component of the reflected signals is the dominant part. Therefore, while the RHCP antenna is an appropriate option for grazing angles altimetry, using a LHCP antenna would be inevitable for higher elevation angles.

The effects of using L1 or L2 carrier frequencies are also investigated. The results from L2 frequency generally show a lower degree of accuracy most likely because of fewer observations (as not all satellites transmit L2C). We combined the L2 sea level products with the L1 products to form L12 measurements for robustness and enhancement. The size of the averaging window also is one of the parameters that affect the accuracy of final products. Longer averaging window improves the quality of the results. The Root Mean Square Error (RMSE) between GNSS-R sea surface heights for LHCP sea-looking antenna with respect to collocated tide gauge measurements are 2.4, 3.0, 4.5, and 5.6 cm for 6, 3, 1, and 0.25-hour window size, respectively.

The investigation of wind effect on the accuracy of GNSS-R sea level measurements reports a lower degree of accuracy during higher wind speeds. The RMSE value of the products can be two times larger in wind speeds above 11 m/s compared to calm sea surface during wind speeds below 2 m/s. However, the final L12 sea level estimates show a remarkable tolerance against high wind speeds, especially for the combined fully-polarimetric solution. The multivariate formulation of the method used in this study shows to be a promising tool for multi-frequency multi-constellation GNSS-R altimetry.

ACKNOWLEDGMENT

The authors would like to thank the editors and three anonymous reviewers for their constructive comments, which significantly improved the presentation and quality of this paper. The German Research Centre for Geosciences (GFZ) is acknowledged for providing the main dataset of this study. The Swedish Meteorological and Hydrological Institute (SMHI) and the Onsala Space Observatory (OSO) are respectively acknowledged for the ancillary data and hosting the experiment.

REFERENCES

[1] K. O. Emery and D. G. Aubrey, *Sea levels, land levels, and tide gauges*. Springer Science & Business Media, 2012, ISBN: 978-1-4613-9101-2.

[2] M. Fernandes, L. Bastos, and M. Antunes, "Coastal satellite altimetry–methods for data recovery and validation," in *3rd meeting of the international gravity and geoid*

commission "Gravity and Geoid. Citeseer, 2002, pp. 26–30.

[3] Martin-Neira, "A passive reflectometry and interferometry system (PARIS): Application to ocean altimetry," *ESA journal*, vol. 17, no. 4, pp. 331–355, 1993.

[4] M. Hoseini, M. Semmling, H. Nahavandchi, E. Rennspiess, M. Ramatschi, R. Haas, J. Strandberg, and J. Wickert, "On the Response of Polarimetric GNSS-Reflectometry to Sea Surface Roughness," *IEEE Transactions on Geoscience and Remote Sensing*, 2020.

[5] M. Hoseini, M. Asgarimehr, V. Zavorotny, H. Nahavandchi, C. Ruf, and J. Wickert, "First evidence of mesoscale ocean eddies signature in GNSS reflectometry measurements," *Remote Sensing*, vol. 12, no. 3, p. 542, 2020.

[6] A. M. Semmling, A. Rösel, D. V. Divine, S. Gerland, G. Stienne, S. Reboul, M. Ludwig, J. Wickert, and H. Schuh, "Sea-ice concentration derived from GNSS reflection measurements in Fram Strait," *IEEE Transactions on Geoscience and Remote Sensing*, vol. 57, no. 12, pp. 10 350–10 361, 2019.

[7] M. Rajabi, H. Nahavandchi, and M. Hoseini, "Evaluation of CYGNSS Observations for Flood Detection and Mapping during Sistan and Baluchestan Torrential Rain in 2020," *Water*, vol. 12, no. 7, p. 2047, 2020.

[8] M. Asgarimehr, M. Hoseini, M. Semmling, M. Ramatschi, A. Camps, H. Nahavandchi, R. Haas, and J. Wickert, "Remote Sensing of Precipitation Using Reflected GNSS Signals: Response Analysis of Polarimetric Observations," *IEEE Transactions on Geoscience and Remote Sensing*, pp. 1–12, 2021.

[9] G. Foti, C. Gommenginger, and M. Srokosz, "First Spaceborne GNSS-Reflectometry Observations of Hurricanes From the UK TechDemoSat-1 mission," *Geophysical Research Letters*, vol. 44, no. 24, pp. 12–358, 2017.

[10] S. Tabibi, "Snow depth and soil moisture retrieval using SNR-based GPS and GLONASS multipath reflectometry," Ph.D. dissertation, University of Luxembourg, Luxembourg, 2016.

[11] K. D. Anderson, "Determination of water level and tides using interferometric observations of GPS signals," *Journal of Atmospheric and Oceanic Technology*, vol. 17, no. 8, pp. 1118–1127, 2000.

[12] F. Soulat, M. Caparrini, O. Germain, P. Lopez-Dekker, M. Taani, and G. Ruffini, "Sea state monitoring using coastal GNSS-R," *Geophysical Research Letters*, vol. 31, no. 21, 2004.

[13] J. Löfgren, R. Haas, H.-G. Scherneck, and M. Bos, "Three months of local sea level derived from reflected GNSS signals," *Radio Science*, vol. 46, no. 6, 2011.

[14] J. S. Löfgren and R. Haas, "Sea level measurements using multi-frequency GPS and GLONASS observations," *EURASIP Journal on Advances in Signal Processing*, vol. 2014, no. 1, pp. 1–13, 2014.

[15] J. Strandberg, T. Hobiger, and R. Haas, "Improving GNSS-R sea level determination through inverse modeling of SNR data," *Radio Science*, vol. 51, no. 8, pp. 1286–1296, 2016.

[16] K. M. Larson, R. D. Ray, and S. D. Williams, "A 10-year comparison of water levels measured with a geodetic GPS receiver versus a conventional tide gauge," *Journal of Atmospheric and Oceanic Technology*, vol. 34, no. 2, pp. 295–307, 2017.

[17] F. Geremia-Nievinski, T. Hobiger, R. Haas, W. Liu, J. Strandberg, S. Tabibi, S. Vey, J. Wickert, and S. Williams, "SNR-based GNSS reflectometry for coastal sea-level altimetry: results from the first IAG inter-comparison campaign," *Journal of Geodesy*, vol. 94, no. 8, pp. 1–15, 2020.

[18] S. Tabibi, F. Geremia-Nievinski, O. Francis, and T. van

Dam, "Tidal analysis of GNSS reflectometry applied for coastal sea level sensing in antarctica and greenland," *Remote Sensing of Environment*, vol. 248, p. 111959, 2020.

[19] A. Santamaría-Gómez and C. Watson, "Remote leveling of tide gauges using GNSS reflectometry: case study at Spring Bay, Australia," *GPS solutions*, vol. 21, no. 2, pp. 451–459, 2017.

[20] A. Padokhin, G. Kurbatov, M. Nazarenko, and V. Smolov, "GNSS Reflectometry of the Black Sea level in the experiments at the Stationary Oceanographic Platform," *Moscow University Physics Bulletin*, vol. 73, no. 4, pp. 422–427, 2018.

[21] A. Alonso-Arroyo, A. Camps, H. Park, D. Pascual, R. Onrubia, and F. Martín, "Retrieval of significant wave height and mean sea surface level using the GNSS-R interference pattern technique: Results from a three-month field campaign," *IEEE Transactions on Geoscience and Remote Sensing*, vol. 53, no. 6, pp. 3198–3209, 2014.

[22] N. Rodriguez-Alvarez, X. Bosch-Lluis, A. Camps, I. Ramos-Perez, E. Valencia, H. Park, and M. Vall-Llossera, "Water level monitoring using the interference pattern GNSS-R technique," in *2011 IEEE International Geoscience and Remote Sensing Symposium*. IEEE, 2011, pp. 2334–2337.

[23] W. Hongguang, K. Shifeng, and Z. Qinglin, "A model for remote sensing sea level with GPS interferometric signals using RHCP antenna," in *ISAPE2012*. IEEE, 2012, pp. 624–626.

[24] A. M. Semmling, G. Beyerle, R. Stosius, G. Dick, J. Wickert, F. Fabra, E. Cardellach, S. Ribó, A. Rius, A. Helm *et al.*, "Detection of Arctic ocean tides using interferometric GNSS-R signals," *Geophysical Research Letters*, vol. 38, no. 4, 2011.

[25] W. Liu, J. Beckheinrich, M. Semmling, M. Ramatschi, S. Vey, J. Wickert, T. Hobiger, and R. Haas, "Coastal sea-level measurements based on GNSS-R phase altimetry: A case study at the Onsala Space Observatory, Sweden," *IEEE Transactions on Geoscience and Remote Sensing*, vol. 55, no. 10, pp. 5625–5636, 2017.

[26] F. Fabra, E. Cardellach, A. Rius, S. Ribó, S. Oliveras, O. Nogués-Correig, M. B. Rivas, M. Semmling, and S. D'Addio, "Phase altimetry with dual polarization GNSS-R over sea ice," *IEEE Transactions on Geoscience and Remote Sensing*, vol. 50, no. 6, pp. 2112–2121, 2011.

[27] L. Bao, N. Wang, and F. Gao, "Improvement of Data Precision and Spatial Resolution of cGNSS-R Altimetry Using Improved Device With External Atomic Clock," *IEEE Geoscience and Remote Sensing Letters*, vol. 13, no. 2, pp. 207–211, 2015.

[28] M. Rajabi, A. Amiri-Simkooei, H. Nahavandchi, and V. Nafisi, "Modeling and prediction of regular ionospheric variations and deterministic anomalies," *Remote Sensing*, vol. 12, no. 6, p. 936, 2020.

[29] M. Rajabi, A. Amiri-Simkooei, J. Asgari, V. Nafisi, and S. Kiaei, "Analysis of TEC time series obtained from global ionospheric maps," *Journal of Geomatics Science and Technology*, vol. 4, no. 3, pp. 213–224, 2015.

[30] M. Semmling, "Altimetric monitoring of Disko Bay using interferometric GNSS observations on L1 and L2," Ph.D. dissertation, Deutsches GeoForschungsZentrum GFZ Potsdam, 2012.

[31] K. M. Larson, E. E. Small, E. Gutmann, A. Bilich, P. Axelrad, and J. Braun, "Using GPS multipath to measure soil moisture fluctuations: initial results," *GPS solutions*, vol. 12, no. 3, pp. 173–177, 2008.

[32] P. Vaníček, "Further development and properties of the spectral analysis by least-squares," *Astrophysics and Space Science*, vol. 12, no. 1, pp. 10–33, 1971.

[33] N. R. Lomb, "Least-squares frequency analysis of un-

equally spaced data," *Astrophysics and space science*, vol. 39, no. 2, pp. 447–462, 1976.

[34] J. D. Scargle, "Studies in astronomical time series analysis. II-Statistical aspects of spectral analysis of unevenly spaced data," *The Astrophysical Journal*, vol. 263, pp. 835–853, 1982.

[35] A. R. Amiri-Simkooei, C. C. Tiberius, and P. J. Teunissen, "Assessment of noise in GPS coordinate time series: methodology and results," *Journal of Geophysical Research: Solid Earth*, vol. 112, no. B7, 2007.

[36] A. Amiri-Simkooei and J. Asgari, "Harmonic analysis of total electron contents time series: methodology and results," *GPS solutions*, vol. 16, no. 1, pp. 77–88, 2012.

[37] A. Amiri-Simkooei, "On the nature of GPS draconitic year periodic pattern in multivariate position time series," *Journal of Geophysical Research: Solid Earth*, vol. 118, no. 5, pp. 2500–2511, 2013.

[38] A. M. Semmling, V. Leister, J. Saynisch, F. Zus, S. Heise, and J. Wickert, "A phase-altimetric simulator: Studying the sensitivity of Earth-reflected GNSS signals to ocean topography," *IEEE Transactions on Geoscience and Remote Sensing*, vol. 54, no. 11, pp. 6791–6802, 2016.

Mahmoud Rajabi graduated in Geodesy and geomatics from the University of Isfahan, Iran. He is currently PhD student at the Norwegian University of Science and Technology (NTNU). His research interests include atmospheric, ocean and land Remote Sensing using Mono- and Bi-static radar systems. His current research focuses on the monitoring of the ocean and land using both ground-based and space-borne GNSS-Reflectometry .

Mostafa Hoseini Mostafa Hoseini graduated in geodesy from the University of Tehran, Tehran, Iran. He has worked for several institutions as a GNSS Engineer in the field of positioning and navigation. Before starting his Ph.D. studies in 2018 at the Norwegian University of Science and Technology (NTNU), Trondheim, Norway, he worked on the analysis of GNSS atmospheric products at the German Research Centre for Geosciences (GFZ), Potsdam, Germany. His research interest includes GNSS-based sensors and techniques for remote sensing applications. His research interest also includes the monitoring of the ocean and Arctic using GNSS-Reflectometry onboard CubeSats. .

Hossein Nahavandchi received the Ph.D. degree from the Royal Institute of Technology (KTH), Stockholm, Sweden in 1998. He is currently a Professor of Geodesy and Geophysics with the Norwegian University of Science and Technology (NTNU), Trondheim, Norway. His research interests involve Global Geodetic Observations System (GGOS) including satellite gravimetry, satellite altimetry, satellite radar interferometry and GNSS to understand the dynamic Earth system by quantifying Earth's change in space and time.

Maximilian Semmling graduated in physics from Leipzig University, Leipzig, Germany, in 2007. He received the Ph.D. degree from Technische Universität Berlin, Berlin, Germany, in 2012. For his doctoral and post-doctoral studies, he was with the German Research Centre for Geosciences (GFZ), Potsdam, Germany, the Institute for Space Studies of Catalonia (IEEC), Barcelona, Spain, and the University of the Littoral Opal Coast (ULCO), Dunkirk, France. In 2020, he joined the Observation Department, German Aerospace Center (DLR), Institute for Solar-Terrestrial Physics, Neustrelitz, Germany. He is experienced in GNSS for Earth observation with a research focus on ocean altimetry and sea ice remote sensing. His work concentrates on the influence of atmosphere and space weather. Corresponding methods cover a wide range from ground-based measurements over maritime, and airborne to satellite platforms..

Markus Ramatschi received the Dipl.-rer. nat. in geophysics and the Ph.D. degree in geophysics from the Technical University of Clausthal, Clausthal-Zellerfeld, Germany, in 1992 and 1998, respectively. He is currently a Senior Scientist at the German Research Centre for Geosciences (GFZ), Potsdam, Germany. His research interests include the operation of a global GNSS sensor station network.

Mehdi Goli is an assistant professor of geodesy at the Faculty of Civil and Architectural Engineering, Shahrood University of Technology, Iran. He received his PhD degrees in geodesy from K. N. Toosi University of Technology, Iran. His research interests focus on space geodesy and geoid determination methods.

Rüdiger Haas is a full professor for space geodesy at the Department of Space, Earth and Environment at Chalmers University of Technology, Sweden. He received his MSc and his PhD degrees in geodesy from Bonn University, Germany. He is the head of the research group for space geodesy at Chalmers and responsible for the geoscience activities at the Onsala Space Observatory. His research interests focus primarily on space geodetic techniques, such as Global Navigation Satellite Systems (GNSS), including GNSS reflectometry, and Very Long Basline Interferometry (VLBI).

Jens Wickert received the graduate degree in physics from the Technical University Dresden, Germany, in 1989, and the Ph.D.degree in geophysics/meteorology from the Karl-Franzens-University Graz, Austria, in 2002. He currently holds a joint professorship of GFZ with the Technical University of Berlin on GNSS remote sensing, navigation and positioning. He is also the Deputy GFZ Section Head Space Geodetic Techniques and the GFZ Research Topic Director "The Atmosphere in Global Change". He has authored/co-authored around 250 ISI listed publications on GNSS Earth observation. He was Principal Investigator of the pioneering GPS radio occultation experiment aboard the German CHAMP satellite and coordinates numerous research projects on GNSS remote sensing.